Cumhuriyet Science Journal

e-ISSN: 2587-246X
ISSN: 2587-2680

Cumhuriyet Sci. J., 42(3) (2021) 586-592
http://dx.doi.org/10.17776/csj.840132

# Structural analysis of pure $PtCu_3$ nanoparticles synthesized by modified Polyol process

***Doğan KAYA*** [1,*]

[1] *Çukurova University, Vocational School of Adana, Department of Electronics and Automation, 01160, Adana / TURKEY*

## Abstract

The development of effective multi-functional Pt-based nanoparticles (NPs) with enhanced activity, stability, and reduced cost for advanced applications still remains a challenge. In this study, $Pt(acac)_2$ and $Cu(OAc)_2$ metal precursors were reduced to form Pt-Cu NPs at 140 °C in ethylene glycol and sodium borohydride that is a secondary reducing agent in the modified polyol method. The x-ray diffraction (XRD) and Rietveld refinement analyses confirmed the face-centered cubic $PtCu_3$ structure with the space groups of $Fm\bar{3}m$ and a lattice constant of $a$=$b$=c=3.6829 Å. The average crystal size was found to be 2.76 nm by Scherrer's formula. Scanning electron microscopy (SEM) images confirm the formation of monodisperse $PtCu_3$ NPs with an average size of 8.04 nm within a narrow range of 5-13 nm. While energy-dispersive x-ray spectroscopy (EDS) analysis confirmed that the composition is formed of 26% Pt and 74% Cu atoms and XRD and EDS analyses were confirmed impurity, by-products, and oxidation free NPs formation.

## Article info

*History:*
Received: 13.12.2020
Accepted: 24.06.2021

*Keywords:*
$PtCu_3$ NP,
Modified polyol process,
Structural properties

## 1. Introduction

Platinum group metals (PGM), that are Pt, Pd, Rh, Ir, Ru, and Os, have attracted enormous interests due to their wide range of applications in catalysis [1], fuel cells and metal winning electrodes [2], dental alloys [3], and even semiconductors [4]. Among these groups, commercially available Pt NPs provided enhanced structural and catalytic activities for catalytic converters in automobiles and fuel cell production methods due to their low environmental pollution, low operating temperatures, and high energy conversion factor [5-7]. Today's biggest problems of Pt catalysis are high cost, mining difficulties, and running out of resources. So there should be an immediate solution to reduce the cost of Pt-based highly active catalytic materials. Recent studies showed that loading Pt metal with other non-precious metals such as Fe, Co, Ni, Cu, etc. enhanced electronic and electro-catalytic properties [8, 9] for oxygen reduction reaction (ORR), ethanol oxidation reactions (EOR), and hydrogenation reactions for fuel cells [10-13]. Reduction of Pt and Cu precursors to form Pt-Cu NPs via chemical synthesis process usually results in three different compositions that are $Pt_3Cu$, PtCu, and $PtCu_3$ [14, 15]. These results also showed that increasing Cu content results in a decrease unit volume so that a more dense crystal structure is formed. The results of the structural analysis showed that $Pt_3Cu$ phase: $Fm\bar{3}m$; a=3.852 Å (ICDD # 04-017-6718), PtCu phase: $Fm\bar{3}m$; a=3.7960 Å (JCPDS #48-1549), and $PtCu_3$ phase: $Pm\bar{3}m$; a=3.692 Å (ICDD #03-065-3247). Additionally comparing methanol oxidation catalytic activities of $Pt_3Cu$, PtCu, and $PtCu_3$ NPs (5.43, 6.96, and 8.65 mA/cm$^2$, respectively) with commercial Pt NPs (1.14 mA/cm$^2$) indicated that increasing Cu ratio in Pt-Cu alloy enhanced electro-oxidation ability [14]. Therefore, $PtCu_3$ alloy becomes a more interesting material to investigate and study the structural and morphological properties for catalytic applications.

Preparing desired pure Pt and Pt-based materials are possible with various methods, such as magnetron sputtering, sol-gel process, polyol process, reverse micelles, thermal decomposition, hydrothermal routes [16-22]. Although all these methods provide a well-controlled composition, size, and shape, the polyol process has been a versatile process to synthesis pure, alloyed, core-shell Pt-based NPs with small sizes [23]. To achieve the desired composition, size, and shape in this process, chemical ingredients, such as surfactants, reducing, and capping agents are highly crucial to form chemically stable and oxidation-free NPs. In the literature, there are plenty of studies on the synthesis

*Corresponding author. *e-mail address: dogankaya@cu.edu.tr*

and structural analysis of PtCu-based alloys [24]. Choosing precursor, surfactant, solvent, reducing agent, additive, annealing temperature and time controls the morphological properties, such as particle size, shape, and crystalline structure. There are different PtCu nanoalloys structures, such as nanoframes, nanowires, spherical, triangular, hexapod, octahedral, hallow nanocages, hierarchical dendrites branched, nanodendrites, etc. with size varies from 2.4 nm to 109 nm [24]. Among these synthesis methods and structures, the nanoalloy size is mostly over 10 nm and there are a few studies, which are mostly for nanowires, reduced the nanoalloy size between 2.4 nm to 5 nm [25, 26]. For example, stabilizing the pH level of the mixture around 9.5-10 with strong bases, such as NaOH or KOH, results in a decrease in the particle size below 7 nm [27, 28]. On the other hand, sodium borohydride ($NaBH_4$) is a secondary reducing agent which was provided successful results for the polyol process of Cu, Ni, Co NPs in ethylene glycol (EG) by slow addition of $NaBH_4$ produced fairly monodisperse isotropic NPs [23]. Capping agent such as oleylamine, oleic acid, or PVP protects the NP from oxidation and provide long term chemical durability in time and led to form cubic, or spherical particle formation, respectively [29-31].

The Pt-Cu NPs were synthesized using a modified polyol process that has been previously employed for various Pt alloys. In this work, low cost, structurally stable, and oxidation-free Pt-Cu NPs was synthesized by controlling amount of solvents, reducing agents, and surfactants which modify the particle size, structure, and morphology. Choosing suitable and optimized additives ratios resulted in the formation of $PtCu_3$ NPs. Following, the structural and morphological properties of as-prepared Pt-Cu NPs were determined by x-ray diffraction (XRD), scanning electron microscopy (SEM), energy-dispersive x-ray spectroscopy (EDS), and Rietveld refinement analyses. The structural analysis showed that the size of $PtCu_3$ NPs was below 10 nm and free from the possible by-products such as impurities and oxidations.

## 2. Experimental Method

### 2.1. Materials

The metal precursors of Platinum(II) acetylacetonate ($Pt(acac)_2$, ≥97.0%) and Copper(II) acetate ($Cu(OAc)_2$, ≥98.0%), ethylene glycol (≥99.8%), sodium borohydride ($NaBH_4$ ≥98%), Polyvinylpyrrolidone (PVP, $M_{av}$ 40 000)), N,N-Dimethylformamide (DMF ≥99.8% ), and sodium hydroxide (NaOH ≥98% ), were purchased from Sigma-Aldrich. All chemicals were of analytical grade and used without further purification.

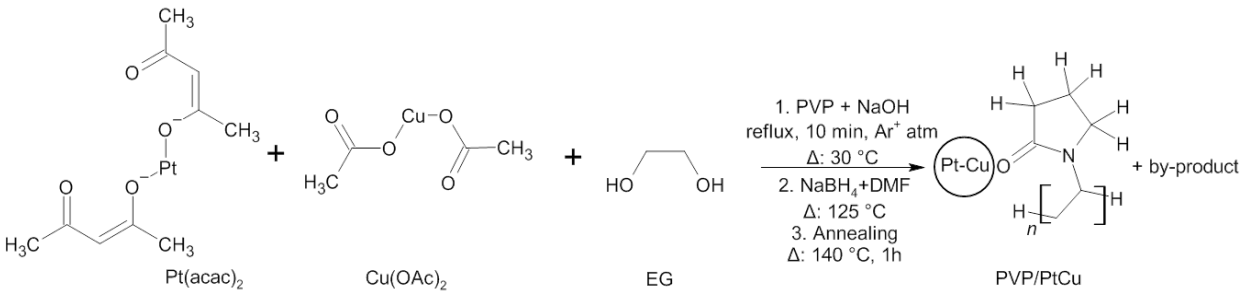


**Figure 1.** Proposed Pt-Cu NP formation mechanism showing reducing $Pt(acac)_2$ and $Cu(OAc)_2$ metal salts with ethylene glycol. The process followed by adding PVP+NaOH at 30 °C under Ar gas flow and $NaBH_4$ at 125 °C, and annealing at 140 °C for 1 h.

### 2.2. Synthesis of Pt–Cu NPs

The proposed Pt-Cu NP formation mechanism was given in Figure 1, 0.77 mmol (0.3041 g) $Pt(acac)_2$ and 0.77 mmol (0.1404 g) $Cu(OAc)_2$ were dissolved in a 50 ml ethylene glycol (EG) and 30 ml DMF under magnetic stirring. The mixture color was bright turquoise. Ingredients were simultaneously added 3.09 mmol (0.1237 g) PVP as a surface agent and 23.19 mmol (0.9279 g) NaOH to stabilize the pH level in the composition (light blue color). Ar gas was bubbled in the fitted condenser during preparation to prevent CuO formation. The mixture temperature started to rise and at 125 °C (green-black color) $NaBH_4$, which was diluted in 50 ml DMF, was slowly injected into the solution. To complete the synthesis, the mixture was annealed at 140 °C for 1 h. The mixture color turned to black which indicates all particles were reduced and then the system cooled down to room temperature via passing tab water around the three-necked bottom flask. Finally, the particles were washed with ethanol and dichloromethane and centrifuged at 9000 rpm for 10 min. The product was dried in an oven at 55 °C for 24 h and used as-prepared before the structural analysis.

### 2.3. Structural characterizations

The phase structure of Pt-Cu NP was determined by a PANalytical XRD system with Cu-$K\alpha$ radiation ($\lambda$=1.54 Å). To determine the structural parameters

FullProf suite was used for Rietveld refinement analysis. SEM images were collected at different places to find average particle size and NP morphology. Collecting EDS data were provided average composition to determine the stoichiometric ratio of Pt-Cu NP.

## 3. Results and Discussions

The structural analysis of the as-prepared Pt-Cu NP was determined by XRD and Rietveld refinement analysis and presented in Figure 2a. Four major diffraction peaks of face-centered-cubic (fcc) of $PtCu_3$ structure (blue circles) match well with that of the standard $PtCu_3$ alloy with the space groups of $Fm\bar{3}m$ (JCPDS No. 35-1358). The peaks at $2\theta$=42.58°, 49.58°, 72.74°, and 88.11° were assigned to the (111), (200), (220), and (311) reflections planes, respectively [14, 32]. Using FullProf suite crystal structure, space group, reflection plane, *d*-space, lattice parameters, and angle of $PtCu_3$ NP structure were obtained by Rietveld refinement analysis and were summarized in Table 1. The simulation patterns (black line), the difference (green line), and Bragg positions (red bars) were presented in Figure 2a. The refinement analysis confirmed the space groups of $Fm\bar{3}m$ of fcc structure and reflection planes for the $PtCu_3$ structure. Figure 2b shows an atomic ball model of the fcc structure of $PtCu_3$ NP obtained by Rietveld refinement analysis. Here the representation of Pt and Cu atoms colored in grey and blue, respectively. The *d*-spaces were found to be 2.12, 1.84, 1.30, and 1.11 Å for the reflection planes of (111), (200), (220), and (311), respectively. The lattice constants and the unit-cell volume were calculated as $a$=$b$=c=3.6829 Å and 49.9539 Å$^3$ which are similar to earlier findings [14]. The crystallite size can be calculated by Scherrer's formula $Dp=K\lambda/(B\cos\theta)$. Here, $Dp$ is the average crystallite size (nm), $K$ is Scherrer constant and varies from 0.68 to 2.08. $K$=0.94 for spherical crystallites with cubic symmetry. $\lambda$ is the wavelength of X-rays, Cu-$K\alpha$=1.54178 Å. $B$ is Full Width at Half Maximum (FWHM) of XRD peak. $\theta$ is Bragg's angle. The average crystal size was calculated to be 2.76 nm for the $PtCu_3$ structure [33]. This XRD analysis showed that $PtCu_3$ NPs successfully synthesized with small crystal size and free from the possible by-products such as impurities and oxidations.

In this study, 50% Pt and 50% Cu precursors were aimed as an entry, however, the $PtCu_3$ structure was obtained via XRD and Rietveld refinement analysis. The chemical synthesis root of NP requires more parameters to control the particle properties such as annealing temperature, annealing time, pH level, precursors, reducing agents, or capping agents. The metal salts were mixed with EG and DMF with a mole ratio of 350 and 100, respectively. Following, PVP and NaOH were added at 30 °C with a mole ratio of 2 and 15, respectively. Finally, $NaBH_4$ was slowly injected with a mole ratio of 24 at 125 °C in 10 min in the mixture under Ar gas atm. The reason for the formation of $PtCu_3$ NP is due to the earlier reduction stage of Cu during the synthesis process. The formation of pure Cu and Pt NPs dissolved in EG and used PVP and $NaBH_4$ during the modified polyol process is mostly developed above 100 °C and 140 °C, respectively [23].

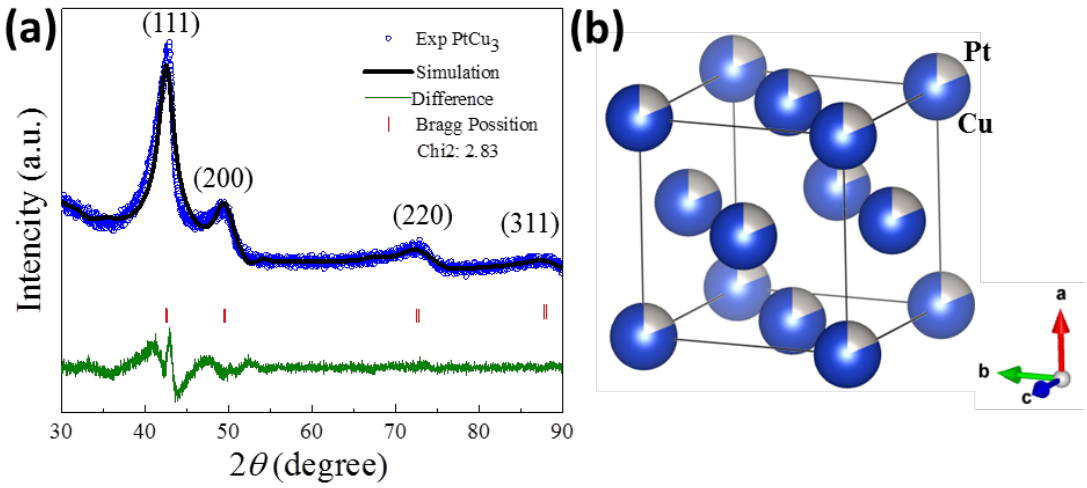


**Figure 2.** (a) X-ray diffraction profiles of $PtCu_3$ NP (blue circles) show the major peaks of [110], [100], and [111] directions. Rietveld refinement analysis: calculated patterns (black line), the difference plot (green line), and Bragg positions (red bars). (b) Atomic ball model of fcc structure of $PtCu_3$ NP obtained by Rietveld refinement analysis.

**Table 1.** Crystal structure, Space group, Reflection plane, *d*-space, Lattice parameter, and Angle of $PtCu_3$ NP structure obtained by Rietveld refinement analysis.

| Crystal Structure | Space Group | Reflection plane | *d*-space (Å) | Lattice Parameter (Å) | Angle (°) |
|---|---|---|---|---|---|
| fcc | $Fm\bar{3}m$ | (111), (200), (220), (311) | 2.12, 1.84, 1.30, 1.11 | $a=b=c=3.6829$ | $\alpha=\beta=\gamma=90°$ |

The morphology and surface structure of the as-prepared $PtCu_3$ NP were characterized by SEM. Figure 3a and b shows a typical surface image of the NPs with a magnification of x200000 and x400000, respectively. Uniform particle distribution is obtained without aggregation on the surfaces. The average particle size was determined by SEM images and binned in 0.5 nm as seen in Figure 3c. The average size of the NPs was found to be $d_0$=8.04 ± 0.08 nm by fitting the histogram as a function of particle size with the log-normal distribution (blue line) in Figure 3d. Here, $\delta$ is the log standard deviation and $d_0$ is the median diameter of $PtCu_3$ NPs. In literature, the smallest sizes of 4.8 nm was obtained for spherical PtCu nanoparticles with using $H_2PtCl_6$ and $Cu(NO_3)_2$ precursors, Ndimethylformamide, oleylemine, and hexadecyltrimethyl ammonium bromide agents and annealed at 170 °C for 24 min [34]. In this study, monodisperse ~8 nm of PtCu nanoalloy synthesis was achieved. Crystallite size can be determined by the peak of XRD which corresponds to the single crystal within a polycrystalline nanoparticle or the size of the grains of a powder sample [35]. Therefore, the crystalline size is expected to be lower than the average particle size of nanoparticles. In this study, we calculated the crystal size to be 2.76 nm which is three times smaller than the average particle size of 8.04 nm. It can be said that there are multicrystalline formation in an average particle.

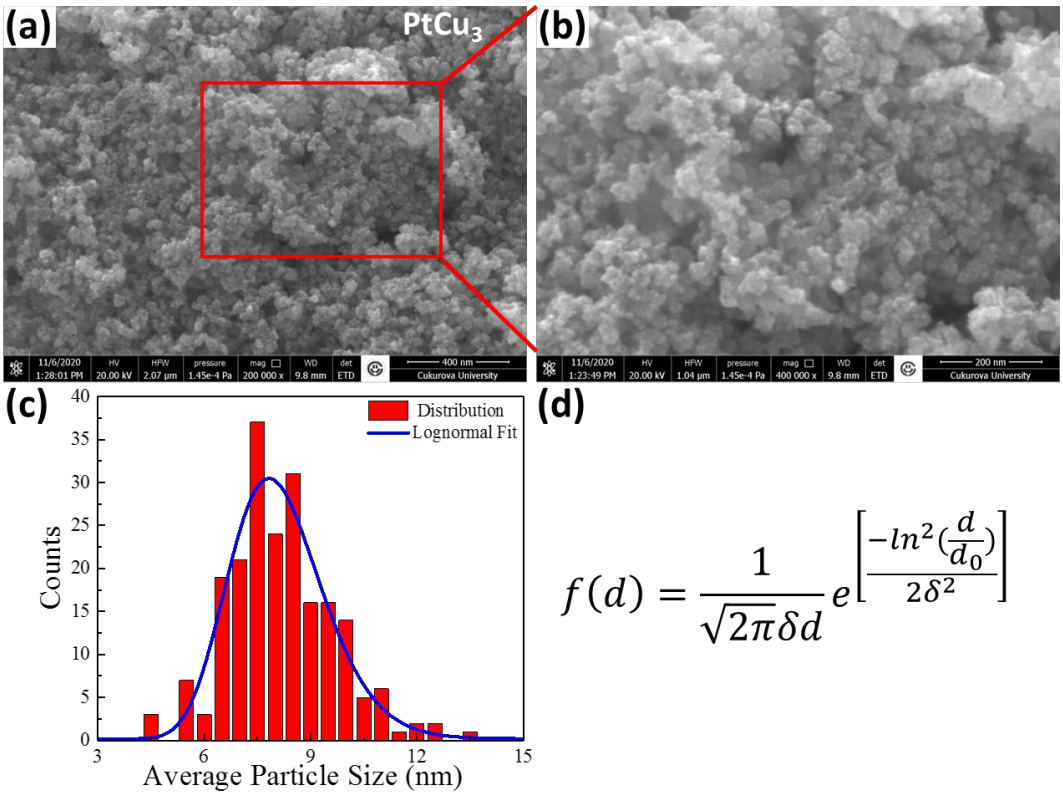


$$f(d) = \frac{1}{\sqrt{2\pi}\delta d} e^{\left[\frac{-ln^2(\frac{d}{d_0})}{2\delta^2}\right]}$$

**Figure 3.** SEM images analysis of $PtCu_3$ NP. (a) The surface morphology of the particles with a magnification of 200000. (b) A selected area from (b). (c) The size distribution of $PtCu_3$ NPs (red bar) with the log-normal fit (blue line) and (d) formula.

To determine atomic composition of as-prepared Pt-Cu NPs, EDS analysis was performed on different areas and collected the average atomic composition percentage. Figure 4a and b show intensity as a function of energy plot and selected point where the EDS data collected. The major Cu and Pt peaks observed in the spectra as well as C and O peaks which are mostly arise form carbon tape used to stabilize particles and surface agents used during preparation. The inset table collected the average atomic composition of detected atoms in Figure 4a. The structure composition ratio was found to be 1:2.8 for Pt:Cu via stoichiometric calculation. This $PtCu_{2.8}$ ratio is quite similar with findings by Rietveld refinement analysis results. The reason of the formation of $PtCu_3$ NPs, reducing $Pt^{2+}$ and $Cu^{2+}$ ions in the mixture EG was used and the $Cu^{2+}$ ions reduce much faster than $Pt^{2+}$ ions and Pt atoms surrounded by Cu atoms instead of binding with other $Cu^{2+}$ ions. For this structure there are 12 Cu atom enclose a Pt atom and 4 Pt atoms bind with a Cu atom [14].

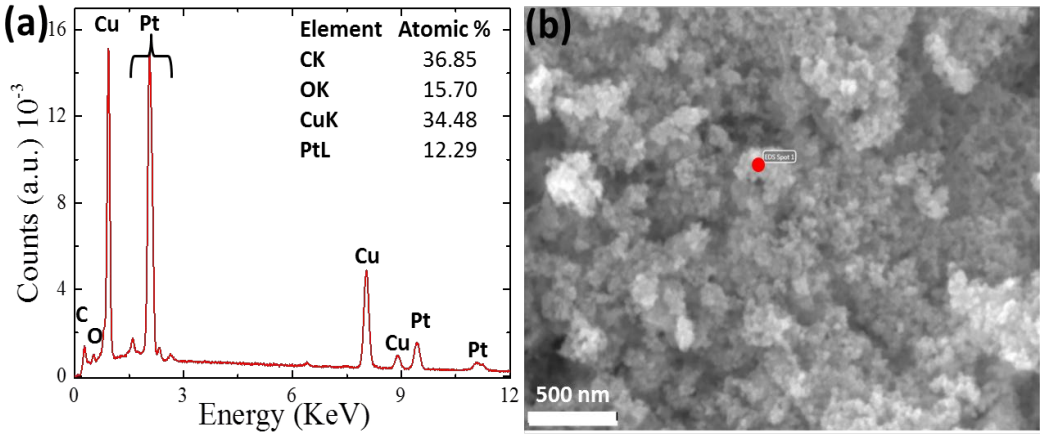


**Figure 4.** (a) EDS analysis of as-prepared $PtCu_3$ NPs with major Cu and Pt as well as C and O peaks. The inset table collected the average atomic composition of detected atoms. (b) SEM image of EDS spot on the surface.

## 4. Conclusion

In conclusion, bimetallic $PtCu_3$ NP was synthesized via the modified polyol process in which EG and $NaBH_4$ used initial and secondary reducing agents, respectively. The particles were reduced to 140 °C under an Argon gas environment to prevent unwanted oxidation formation. Using PVP as a surface capping agent also vastly improved the particle protection from oxidation and provides chemical stability. The structural formation of $PtCu_3$ NPs was first determined by XRD and Rietveld refinement analysis in that were confirmed the $Fm\bar{3}m$ space group with a lattice constant of $a$=$b$=c=3.6829 Å. The crystal size of $PtCu_3$ NPs was determined by FHWM of the XRD peaks and calculated as 2.76 nm using Scherrer's formula. Following the average size of $PtCu_3$ was 8.04 nm via SEM images. The structural composition was found to be 1:2.8 for Pt:Cu confirmed by EDS with oxidation and impurity-free compositions.

## Acknowledgement

I would like to thank Prof.Dr. Faruk Karadag and Assoc.Prof. Ahmet Ekicibil for valuable discussions.

## Conflict of interest

The authors declare that they have no conflict of interests.

## References


[1] Wang X.X., Swihart M.T., Wu G., Achievements, challenges and perspectives on cathode catalysts in proton exchange membrane fuel cells for transportation, *Nat. Catal.,* 2(7) (2019) 578-589.

[2] Pivovar B., Catalysts for fuel cell transportation and hydrogen related uses, *Nat. Catal.,* 2(7) (2019) 562-565.

[3] Colic M., Stamenkovic D., Anzel I., Lojen G., Rudolf R., The influence of the microstructure of high noble gold-platinum dental alloys on their corrosion and biocompatibility in vitro, *Gold Bull.,* 42(1) (2009) 34-47.

[4] Ben Saber N., Mezni A., Alrooqi A., Altalhi T., A review of ternary nanostructures based noble metal/semiconductor for environmental and renewable energy applications, *J. Mater. Res. Technol.,* 9(6) (2020) 15233-15262.

[5] Xia B.Y., Wu H.B., Yan Y., Lou X.W., Wang X., Ultrathin and Ultralong Single-Crystal Platinum Nanowire Assemblies with Highly Stable Electrocatalytic Activity, *J. Am. Chem. Soc.,* 135(25) (2013) 9480-9485.

[6] Wang J., Barriers of scaling-up fuel cells: Cost, durability and reliability, *Energy,* 80 (2015) 509-521.

[7] Chen Y., Zhang G., Ma J., Zhou Y., Tang Y., Lu T., Electro-oxidation of methanol at the different carbon materials supported Pt nano-particles, *Int. J. Hydrogen Energy,* 35(19) (2010) 10109-10117.

[8] Zaleska-Medynska A., Marchelek M., Diak M., Grabowska E., Noble metal-based bimetallic nanoparticles: the effect of the structure on the optical, catalytic and photocatalytic properties, *Adv. Colloid Interface Sci.,* 229 (2016) 80-107.

[9] Srinoi P., Chen Y.-T., Vittur V., Marquez M., Lee T., Bimetallic Nanoparticles: Enhanced Magnetic and Optical Properties for Emerging Biological Applications, *Appl. Sci.,* 8 (2018) 1106.

[10] Li C.-H., Li M.-C., Liu S.-P., Jamison A.C., Lee D., Lee T.R., Lee T.-C., Plasmonically Enhanced Photocatalytic Hydrogen Production from Water: The Critical Role of Tunable Surface Plasmon Resonance from Gold–Silver Nanoshells, *ACS Appl. Mater. Interfaces,* 8(14) (2016) 9152-9161.

[11] Hien Pham T.T., Cao C., Sim S.J., Application of citrate-stabilized gold-coated ferric oxide composite nanoparticles for biological separations, *J. Magn. Magn. Mater.,* 320(15) (2008) 2049-2055.

[12] Li X., Liu H., Liu S., Zhang J., Chen W., Huang C., Mao L., Effect of Pt–Pd hybrid nano-particle on CdS's activity for water splitting under visible light, *Int. J. Hydrogen Energy,* 41(48) (2016) 23015-23021.

[13] Farahmandjou M., Effect of Oleic Acid and Oleylamine Surfactants on the Size of FePt Nanoparticles, *J. Supercond. Novel Magn.,* 25(6) (2012) 2075-2079.

[14] Jia Y., Cao Z., Chen Q., Jiang Y., Xie Z., Zheng L., Synthesis of composition-tunable octahedral Pt–Cu alloy nanocrystals by controlling reduction kinetics of metal precursors, *Sci. Bull.,* 60 (2015).

[15] Saravanan G., Khobragade R., Chand Nagar L., Labhsetwar N., Ordered intermetallic Pt–Cu nanoparticles for the catalytic CO oxidation reaction, *RSC Adv.,* 6(88) (2016) 85634-85642.

[16] Vernieres J., Steinhauer S., Zhao J., Chapelle A., Menini P., Dufour N., Diaz R.E., Nordlund K., Djurabekova F., Grammatikopoulos P., Sowwan M., Gas Phase Synthesis of Multifunctional Fe-Based Nanocubes, *Adv. Funct. Mater.,* 27(11) (2017) 1605328.

[17] Salavati-Niasari M., Davar F., Mazaheri M., Shaterian M., Preparation of cobalt nanoparticles from [bis(salicylidene)cobalt(II)]–oleylamine complex by thermal decomposition, *J. Magn. Magn. Mater.,* 320(3) (2008) 575-578.

[18] Gul I.H., Maqsood A., Structural, magnetic and electrical properties of cobalt ferrites prepared by the sol–gel route, *J. Alloys Compd.,* 465(1) (2008) 227-231.

[19] Shemer G., Tirosh E., Livneh T., Markovich G., Tuning a Colloidal Synthesis to Control Co2+ Doping in Ferrite Nanocrystals, *J. Phys. Chem. C.,* 111(39) (2007) 14334-14338.

[20] Millot N., Le Gallet S., Aymes D., Bernard F., Grin Y., Spark plasma sintering of cobalt ferrite nanopowders prepared by coprecipitation and hydrothermal synthesis, *J. Eur. Ceram. Soc.,* 27(2) (2007) 921-926.

[21] Lisiecki I., Pileni M.P., Synthesis of Well-Defined and Low Size Distribution Cobalt Nanocrystals: The Limited Influence of Reverse Micelles, *Langmuir,* 19(22) (2003) 9486-9489.

[22] Meng Q., Zhang Y., Dong P., Use of electrochemical cathode-reduction method for leaching of cobalt from spent lithium-ion batteries, *J. Clean. Prod.,* 180 (2018) 64-70.

[23] Fiévet F., Ammar-Merah S., Brayner R., Chau F., Giraud M., Mammeri F., Peron J., Piquemal J.Y., Sicard L., Viau G., The polyol process: a unique method for easy access to metal nanoparticles with tailored sizes, shapes and compositions, *Chem. Soc. Rev.,* 47(14) (2018) 5187-5233.

[24] Yan W., Zhang D., Zhang Q., Sun Y., Zhang S., Du F., Jin X., Synthesis of PtCu–based nanocatalysts: Fundamentals and emerging challenges in energy conversion, *J. Energy Chem.,* 64 (2022) 583-606.

[25] Fang D., Wan L., Jiang Q., Zhang H., Tang X., Qin X., Shao Z., Wei Z., Wavy PtCu alloy nanowire networks with abundant surface defects enhanced oxygen reduction reaction, *Nano Res.,* 12(11) (2019) 2766-2773.

[26] Liao Y., Yu G., Zhang Y., Guo T., Chang F., Zhong C.-J., Composition-Tunable PtCu Alloy Nanowires and Electrocatalytic Synergy for Methanol Oxidation Reaction, *J. Phys. Chem. C.,* 120(19) (2016) 10476-10484.

[27] Huang K.-C., Ehrman S.H., Synthesis of Iron Nanoparticles via Chemical Reduction with Palladium Ion Seeds, *Langmuir,* 23(3) (2007) 1419-1426.

[28] Li N., Tang S., Meng X., Reduced Graphene Oxide Supported Bimetallic Cobalt–Palladium Nanoparticles with High Catalytic Activity towards Formic Acid Electro-oxidation, *J Mater Sci Technol.,* 31(1) (2015) 30-36.

[29] Arán-Ais R.M., Vidal-Iglesias F.J., Solla-Gullón J., Herrero E., Feliu J.M., Electrochemical Characterization of Clean Shape-Controlled Pt Nanoparticles Prepared in Presence of Oleylamine/Oleic Acid, *Electroanalysis,* 27(4) (2015) 945-956.

[30] Tong Y.Y., Polyvinylpyrrolidone (pvp) for enhancing the activity and stability of platinum-based electrocatalysts, *Google Patents*, 2015.

[31] Cao Y., Yang Y., Shan Y., Huang Z., One-Pot and Facile Fabrication of Hierarchical Branched Pt–Cu Nanoparticles as Excellent Electrocatalysts for Direct Methanol Fuel Cells, *ACS Appl. Mater. Interfaces,* 8(9) (2016) 5998-6003.

[32] Wu F., Niu W., Lai J., Zhang W., Luque R., Xu G., Highly Excavated Octahedral Nanostructures Integrated from Ultrathin Mesoporous PtCu3 Nanosheets: Construction of Three-Dimensional Open Surfaces for Enhanced Electrocatalysis, *Small,* 15(10) (2019) 1804407.

[33] Papa F., Negrila C., Miyazaki A., Balint I., Morphology and chemical state of PVP-protected Pt, Pt–Cu, and Pt–Ag nanoparticles prepared by alkaline polyol method, *J. Nanopart. Res.,* 13(10) (2011) 5057.

[34] Du X., Luo S., Du H., Tang M., Huang X., Shen P.K., Monodisperse and self-assembled Pt-Cu nanoparticles as an efficient electrocatalyst for the methanol oxidation reaction, *J. Mater. Chem. A.,* 4(5) (2016) 1579-1585.

[35] Bishnoi A., Kumar S., Joshi N., Chapter 9 - Wide-Angle X-ray Diffraction (WXRD): Technique for Characterization of Nanomaterials and Polymer Nanocomposites, in: S. Thomas, R. Thomas, A.K. Zachariah, R.K. Mishra (Eds.), Amsterdam: Elsevier, (2017) 313-337.